

Seismic fragility assessment of fire-damaged reinforced concrete frames using probabilistic analysis

Sajjad Mohammadian Abi¹, Mohammad Reza Mansoori^{2*}, Panam Zarfam³

1,2,3- Department of civil engineering, SR.C., Islamic Azad University, Tehran, Iran

Abstract

An increase in temperature during a fire in concrete members causes physical and chemical changes and reduces compressive strength. Therefore, even if the structure remains stable after the fire, evaluating its seismic behavior is of great importance. Accordingly, this study aims to investigate the seismic fragility of reinforced concrete moment frames that have been damaged by fire and have not been repaired or strengthened, using probabilistic and sensitivity analysis methods. For this purpose, a seven-story reinforced concrete frame was first designed, and its thermo-mechanical properties were modeled in OpenSees software. Three fire scenarios lasting one, two, and three hours were applied to the structure. The heat transfer analysis of the beam and column sections damaged during the fire was carried out using Abaqus software. The incremental dynamic analysis and seismic fragility curves of the structure were obtained and compared using both deterministic and probabilistic approaches, considering uncertainties in material properties, gravity load, seismic load, and geometry. The results of these curves show that the probability that the structure will exceed the limit states (IO, LS, and CP) increases as the duration of thermal loading increases. Specifically, the probability of exceedance from the LS limit state at a spectral acceleration of $S_a = 0.9g$ for the no-fire case and for frames exposed to one-, two-, and three-hour fires is 71%, 86%, 90%, and 97%, respectively. The results of the seismic sensitivity analysis indicate that reinforcement yield stress, concrete strength, and reinforcement cover are more seismically sensitive compared to other random variables.

Keywords: Fire, Probabilistic analysis, concrete frame, Sensitivity analysis, Fragility curve, Monte Carlo analysis, Random variable

1. Introduction

Numerous hazards threaten the structural safety of buildings during their service life, including earthquakes, fires, and explosions [1]. Each of these events can cause either local damage or lead to overall structural failure [2]. Among these hazards, seismic loads from earthquakes are the most critical and are a primary consideration in design [3]. Various factors can influence a structure's seismic response, including fire. Fire can reduce structural strength and increase the response under subsequent loads [2]. When a structure is exposed to thermal loads and then subjected to seismic loads without any repair or strengthening, its seismic response may vary significantly [4]. Reinforced concrete structures generally perform better under fire than other types of structures due to their lower thermal conductivity, higher heat capacity, and slower degradation of

mechanical properties. However, severe and prolonged fire can cause significant structural damage. Unlike the obvious severe damage to concrete and substantial loss of cross-sectional area, which clearly indicate serious harm, the reduction in structural performance of reinforced concrete elements due to chemical changes in material layers may not be immediately evident. Therefore, even if the structure remains stable after the fire has been completely extinguished, it is crucial to evaluate its seismic behavior. Accordingly, determining the residual capacity of structural members using engineering methods is essential to facilitate reuse or to guide possible strengthening measures in reinforced concrete structures after a fire [5].

The residual capacity of reinforced concrete structural components exposed to fire has been extensively studied by researchers in recent years. Some studies have focused on the performance of individual structural elements through destructive testing. Li et al. [6] demonstrated that the ultimate load-bearing capacity, stiffness, ductility, and energy dissipation capacity of reinforced concrete frames decrease after fire exposure. Wang et al. [7] investigated the post-fire seismic behavior of five steel-reinforced concrete (SRC) frames and beams. Their study of hysteresis curves, deformation, stiffness, ductility, and damping ratio of SRC frames indicated that heat exposure reduces load-bearing capacity. Jia et al. [8] showed that the seismic performance of reinforced concrete structures equipped with metallic yielding dampers (MYD) can be significantly impaired due to fire damage. Jin et al. [9] examined the behavior of reinforced concrete beams and columns under fire, considering progressive collapse scenarios, and found that 90 minutes of heating increases the potential for progressive failure. Sosso et al. [10] reported that, among random variables, concrete cover, reinforcement yield strength, and concrete strength are the most significant uncertainties in probabilistic fire analysis. Aydin et al. [11] found that increasing concrete cover in steel-profile composites enhances compressive strength and reduces crack widths. Van Cao et al. [12] demonstrated that the ultimate load, yield load, and stiffness of concrete-filled steel tubes (CFST) decrease after fire exposure compared to control specimens. Thongchom et al. [13] investigated the behavior of reinforced concrete (RC) and GFRP-RC beams under fire load, showing that RC steel beams exhibit higher fire resistance than GFRP-RC beams. Liu et al. [14] studied the residual flexural behavior of T-shaped composite and monolithic beams after fire exposure and found that residual flexural capacity is lower in composite beams. Li et al. [15] showed that fire exposure of precast concrete columns with grouted sleeve connections shifts failure modes from flexural to shear-flexural or bond-shear failures. Chandra et al. [16] indicated that corrosion significantly affects the fire performance of reinforced concrete columns, although high-strength concrete (HSC) columns perform better under fire loads. Wu et al. [17] reported that self-centering connections exposed to

fire maintain good performance, but fire still significantly impacts the seismic behavior of self-centering concrete connections. Kunawisarut et al. [18] found that strengthening fire-damaged concrete cylinders with jute fiber-reinforced biopolymer composites (JFRB) increases compressive strength by 2.02 to 3.69 times. Wang et al. [19] demonstrated that using fiber cement boards as fire insulation on steel beams may be ineffective because these boards become brittle and prone to fracture at high temperatures. Azadi Kenari et al. [20] reported that elevated temperatures in reinforced concrete (RC) beam-column connections containing natural aggregate (NAC) cause more damage than connections with recycled coarse aggregate (RAC). Zhang et al. [21] showed that replacing part of the cement with steel slag (SSP) in fire-damaged concrete beams has a minor adverse effect on ductility and stiffness in the elastic range.

A review of previous studies indicates that fire-damaged structures exhibit different seismic behavior compared to intact structures. Although the term "post-fire seismic performance" has been used in earlier research, most studies have focused on cyclic loading models, and seismic loads have rarely been directly evaluated using ground motion records. Furthermore, prior studies have examined the mechanical properties of individual structural members, such as beams, columns, and reinforced concrete slabs, whereas the overall response of a frame under fire is considerably more complex and different from that of its individual members. Naturally, this behavioral difference can affect the seismic fragility of various structures. Most prior investigations were conducted experimentally, and in numerical models, only two-story, two-span frames under cyclic loading were analyzed. Previous studies primarily employed deterministic analysis for modeling, where all structural properties and loading were assumed constant. Considering that random variables play a significant role in evaluating the seismic behavior of structures, the reliance on deterministic analysis represents another research gap in prior studies.

In this study, a comprehensive investigation of the seismic fragility of a seven-story reinforced concrete moment frame, which was exposed to fire and subsequently fully extinguished without any repair or strengthening, has been conducted using Monte Carlo probabilistic analysis. The analysis was performed in two sections: considering and not considering random variables, at different performance levels (IO, LS, CP). The random variables considered for the probabilistic analysis include the modulus of elasticity and yield stress of the reinforcement, concrete strength, reinforcement cover, dead and live loads, and span length. To apply seismic loads and perform fragility analysis, twenty-eight near-field ground motion records introduced by FEMA P695 were used in an incremental dynamic analysis (IDA). Evaluating the role and impact of uncertainties on the seismic response sensitivity of the frame using sensitivity analysis represents another innovative

aspect of the present study. A flowchart illustrating the research procedure is presented in Figure 1.

2. Structural model

A seven-story, three-dimensional structure with high ductility, four 6-meter spans, and a square plan is considered. For the design, the structure is assumed to be located in a high seismic zone ($A = 0.3g$) on type III soil. The dead load is taken as 600 kg/m^2 , and the live load as 200 kg/m^2 . The Iranian Standard 2800 is used for lateral loading, and the reinforced concrete frame has been designed according to the Iranian Standard for Design of Reinforced Concrete Structures. A 28-day concrete compressive strength of 21 MPa, reinforcement with a yield stress of 400 MPa, and an elastic modulus of $2 \times 10^5 \text{ MPa}$ have been used for the design of this frame. The results of the structural design based on reinforced concrete sections are presented in Table 1. In this table, H represents the cross-sectional dimension in centimeters, and T represents the diameter of the reinforcement in millimeters.

2.1. Modelling thermo-mechanical properties of structure

After the initial design, the middle frame of the structure was selected for the thermo-mechanical analysis, and OpenSees [22] software was used for thermo-mechanical modeling. Figure 2 shows the finite element model of the two-dimensional frame. Various scenarios are available for the seismic evaluation of fire-damaged frames, in which different stories may be affected by fire. In this study, it is assumed that the structure undergoes a fire incident on one of its floors, and the selection process of the floor subjected to fire is explained in Section 4. Therefore, the concentrated plastic hinge model (Figure 2) was used in the nonlinear modeling for all spans except those on the fire-affected floor. To define the concentrated plastic hinge, two coincident points were determined and connected using a zero-length element, and elastic elements were combined with elements possessing concentrated plasticity properties. For this purpose, the *ModIMKPeakOriented* material (Figure 3) was used to define the flexural plastic hinge.

For all beams and columns (in floors without fire), elastic elements were used, and all plastic properties were summarized in the hinges. However, on the fire-affected floor where thermal loading is applied, distributed plasticity was utilized [23]. In the distributed plasticity modeling, *dispBeamColumnThermal* elements with *Concrete02thermal* material were employed for concrete and *Steel02thermal* material for reinforcement. Mechanical properties of these materials, based on the maximum temperature experienced during the fire, are shown in Table 2. In this table, θ represents temperature, $f_{c,\theta}$ is the concrete strength at temperature θ , f_{ck} is the concrete strength at normal temperature, $\varepsilon_{c,\theta}$ is the

concrete strain at temperature θ , $\varepsilon_{cu,\theta}$ is the ultimate concrete strain at temperature θ , $f_{sy,\theta}$ is the yield stress of reinforcement at temperature θ , f_{yk} is the yield stress of reinforcement at normal temperature, $f_{sp,\theta}$ is the ultimate stress of reinforcement at temperature θ , $E_{s,\theta}$ is the elastic modulus of reinforcement at temperature θ , and E_s is the elastic modulus of steel at normal temperature.

2.2. Fire load

It is typically necessary, when considering thermal loading, to first define a fire scenario and then calculate and apply the corresponding temperature-time curves to the structure. Various temperature-time curves are generated based on the method outlined in EN 1991-1-2 [25] and variations in the wall span lengths, which include windows and doors located in the perimeter walls. Since this research focuses on evaluating the seismic performance and residual capacity of concrete moment-resisting frames that have previously experienced a fire, it is assumed that the temperature of structural elements has returned to ambient levels by the time the earthquake occurs. Therefore, the fire loading considered in this study includes both a heating phase and a cooling phase, ensuring that the frame cools down to ambient temperature after reaching its maximum temperature. To achieve this, the thermal loads decrease linearly after reaching the maximum temperature and enter the cooling phase (Figure 4). Accordingly, fire curves with durations of one, two, and three hours, corresponding to opening factors of 0.067, 0.12, and 0.2, respectively, have been used in this research [26].

2.3. Heat transfer analysis of sections

Heat transfer in a structural member can be divided into two parts: the first is the transfer of heat from the heat source to the exposed surfaces, and the second is the heat flow within the structural member itself. As a result, the temperature varies across the height of the cross-sections in beams and columns. In other words, the surface of the cross-section in direct contact with fire experiences a higher temperature compared to the core. Since OpenSees software does not perform heat transfer analysis for beam and column sections, the cross-sections of the beams and columns located on the fire-affected floor were first modeled and analyzed in Abaqus software [27] to perform the heat transfer analysis and enhance the accuracy of the results. The heat transfer element in Abaqus was used to model heat transfer within the elements. Thermal loads were defined and applied to the boundary points. After meshing and performing the thermal analysis, temperature-time curves at the required points of the cross-sections were extracted and used in OpenSees.

Figure 5 shows the reinforced concrete beam cross-section modeled in Abaqus under thermal loads of one, two, and three hours. Figure 6 presents the temperature–time curves extracted from the bottom reinforcement, the concrete at the bottom of the section, and the concrete at the core of the beam cross-section. As shown, both heating and cooling phases are included in these curves. In OpenSees, each cross-section with thermo-mechanical properties (sections exposed to fire) is divided into nine parts, with a temperature–time curve assigned to each part. These curves for the nine depths of each cross-section were extracted from the heat transfer analysis in Abaqus and incorporated into the finite element model created in OpenSees. The mechanical properties of the concrete and steel materials are updated according to the maximum temperature experienced by each of these nine parts (Table 2).

Although the proposed thermo-mechanical modeling approach provides a powerful framework for simulating the response of reinforced concrete structures to fire, several limitations should be considered. First, in the heat transfer analysis, concrete is assumed to be homogeneous, and phenomena such as cracking, spalling, and moisture migration—which can affect the actual thermal behavior under severe fire conditions—are not accounted for. Second, the thermal properties of materials are defined based on the values provided in the Eurocode, and no calibration was performed using project-specific experimental data. Third, the reinforcement is modeled as independent fibers fully bonded with the concrete, and the potential effects of bond degradation at high temperatures are not considered. Therefore, these limitations should be taken into account when interpreting the results and applying the method in practical design.

2.4. Validation

The study conducted by Qiao [28] was used to validate the thermo-mechanical behavior of the beams. In their experimental work, a reinforced concrete beam was subjected to thermal loading, and its response and heat transfer were evaluated. The concrete compressive strength was 49 MPa, and the yield stress of the reinforcement was 357 MPa. The vertical load applied to the beam was 79 kN. A schematic of Qiao's model is shown in Figure 7. The results of the heat transfer analysis (conducted in Abaqus) and the thermo-mechanical analysis (conducted in OpenSees) show good agreement between the model in this study and Qiao's experimental results. The fire load curve applied to the experimental specimen, along with the temperature-time curves at the mid-section for both Qiao's model and the numerical model of this study, are presented in Figure 8-a. The results of the thermo-mechanical analysis are shown in Figure 8-b.

The experimental model by Gernay et al. [29] was used to validate the thermo-mechanical behavior of a reinforced concrete column. In their study, a column with a concrete compressive strength of 31 MPa and reinforcement yield stress of 500 MPa was subjected to thermal loading, including a cooling phase, and the vertical displacement at the top of the column as well as its fire resistance were evaluated. Their experimental model is shown in Figure 9. The thermal loading in this study is based on the ISO fire curve, as illustrated in Figure 10-a. The supports of the model are assumed to be fixed, and a vertical load of 322 kN is applied at the top of the column in the validation model.

The results of the vertical displacement of the column under fire loading, including the cooling phase, are presented in Figure 10-b. The results show good agreement between Gernay's experimental model and the numerical model developed in this study.

3. Research method

3.1. Fragility analysis

The fragility of a structure is defined as the probability of exceeding an engineering demand parameter (EDP) relative to various allowable conditions (AC) at different levels of seismic intensity (IM) [30].

$$P((EDP > AC) | IM) \quad (1)$$

Therefore, the fragility of the structure can be defined using Equation 7 when evaluating the residual seismic capacity of fire-damaged concrete structures:

$$P((EDP > AC) | Fire, IM) \quad (2)$$

In this study, the maximum floor drift is considered as the EDP, the spectral acceleration (S_a) as the IM, and the thermal loads introduced in Section 2-2 as three fire scenarios. The incremental dynamic analysis (IDA) method has been employed for fragility assessment. Given that near-field and far-field records affect structures differently, this study focuses on near-field records, and the fragility and structural responses are investigated solely under near-field excitations. Accordingly, 28 near-field records from FEMA P695 were used to apply seismic loads and perform the IDA, as presented in Table 3. Each record was scaled from a spectral acceleration of 0.1g in increments of 0.1g until the structure reached instability. A maximum drift of 0.1 was assumed as the criterion for structural instability [31].

The fragility of the structure was investigated using two approaches in this study. Initially, IDA and fragility curves were assessed for fire-damaged structures under earthquake loading using a deterministic method without considering uncertainties. Subsequently, IDA and fragility curves were developed probabilistically by incorporating uncertainties through a sample space. For the probabilistic analysis, a Monte Carlo simulation was performed at each spectral acceleration level, and the cumulative distribution function (CDF) of the maximum drift values was used to construct the IDA curves. Fragility curves for different performance levels were then developed based on these CDF curves. Three performance levels—Immediate Occupancy (IO), Life Safety (LS), and Collapse Prevention (CP)—were considered, with story drift limits at IO, LS, and CP levels, according to FEMA-356 [33], set as 1%, 2%, and 4% of the story height, respectively [34].

3.2. Sensitivity analysis

Sensitivity analysis is a type of probabilistic analysis that examines the effects of variations in one or more random variables on the structural response. For instance, it can evaluate how changes in the yield stress of reinforcement influence the seismic response of fire-damaged frames. Various methods exist for assessing the sensitivity of a structure to specific engineering parameters. Among these, Monte Carlo Simulation (MCS) is one of the most robust approaches for uncertainty and probabilistic analyses [35]. Additionally, MCS is frequently used to validate probabilistic analysis methods.

Three types of random variables are considered in this study: material, loading, and geometric variables. The yield stress of reinforcement (F_y), modulus of elasticity of reinforcement (E), and concrete compressive strength (F_c) are the random variables related to materials. Dead load, live load, and seismic load are considered as random variables for loading. Span length and cover thickness are assumed as random variables associated with geometry [17]. The distribution type and mean value of each variable are summarized in Table 4.

4. Determination of the Fire-Affected Story (Critical Story)

Since the main objective of this study is to evaluate the residual seismic capacity of reinforced concrete structures exposed to fire, and considering that fire can occur on different floors of a multi-story building, it is assumed that the fire takes place on the floor exhibiting the highest dynamic response (inter-story drift). This assumption ensures that the dynamic response of the structure is primarily influenced by the fire. To identify the fire-affected floor, seven records listed in Table 3 were selected, scaled according to the Iranian Standard 2800, and applied to the structure. The structure was then analyzed using

the nonlinear time-history analysis method, and the maximum inter-story drift was extracted and presented in Figure 11.

The maximum drift values of the stories indicate that the fourth floor experiences the highest drifts, with an average maximum drift of 0.026. Since this floor exhibits the largest drift under the seismic loading scenario, it is assumed to be the fire-affected floor for evaluating the seismic behavior of the fire-damaged frame. Consequently, the fire load is applied to the beams and columns of the fourth floor.

Figure 12 shows the hysteresis curves of the steel (reinforcement) and concrete fibers of the beam exposed to fire. The concrete fiber represents the lowest part of the beam exposed to fire, while the steel fiber corresponds to the reinforcement at the bottom of the beam, which is closest to the fire-concrete boundary. According to Figure 12, the longer the materials are exposed to fire, the more both their strength and deformation capacity decrease. In fact, heating and subsequent cooling of the materials cause them to exhibit more brittle behavior while losing strength. Naturally, this reduction in strength results in different seismic behavior for structures damaged by fire compared to structures subjected only to seismic loads. If the frame is damaged by three hours of fire exposure, the strength of the reinforcement under seismic loading is reduced by half. Additionally, the ultimate strength of the concrete occurs at higher strains. In Figure 12, the term EQ-Only refers to a frame subjected only to seismic loads without fire exposure. The term 1H+EQ represents the earthquake applied to a frame damaged by one hour of fire exposure, 2H+EQ corresponds to a frame damaged by two hours of fire exposure, and 3H+EQ indicates a frame damaged by three hours of fire exposure.

5. Evaluation of IDA and fragility curves

The IDA (Incremental Dynamic Analysis) and fragility curves of the frame are presented in this section in two parts: with and without considering random variables, for four scenarios corresponding to the duration of fire exposure that caused damage to the frame. In the first scenario, it is assumed that the frame has not experienced any fire and is merely subjected to seismic loading (EQ-Only). The second scenario involves the seismic evaluation of the residual capacity of the frame damaged by one hour of fire exposure (1H+EQ). In the third scenario, the frame is assumed to have been damaged by two hours of fire exposure (2H+EQ). Finally, in the fourth scenario, the frame is assumed to have experienced three hours of fire exposure (3H+EQ).

5.1. First section: not considering random variables

In this section, the IDA and fragility curves of the structure are examined under deterministic conditions. Therefore, all the parameters introduced in Table 4 are assumed

constant in this scenario, and only seismic loads and their spectral accelerations are considered as variables. The IDA and fragility curves are presented for four cases: EQ-Only, 1H+EQ, 2H+EQ, and 3H+EQ. Figure 13 shows the IDA curves of the structure under the 28 earthquake records listed in Table 3 for the four aforementioned cases.

The primary application of IDA curves is to evaluate the probability of structures exceeding different performance levels. In this study, three limit states—Immediate Occupancy (IO), Life Safety (LS), and Collapse Prevention (CP)—were used to assess the fragility curves. Figure 14 presents the fragility curves of the structure for different fire exposure durations under these three limit states. The evaluation of the fragility curves for the scenarios EQ-Only, 1H+EQ, 2H+EQ, and 3H+EQ shows that fire-induced damage negatively affects the probability of exceeding performance levels. The longer the fire exposure, the higher the exceedance probability under seismic loading. The fragility curves indicate that the exceedance probability at the IO performance level under a spectral acceleration of $S_a=0.5g$ is 49% for the EQ-Only scenario. For the 1H+EQ, 2H+EQ, and 3H+EQ scenarios, the exceedance probability at this limit state increases to 50%, 86%, and 100%, respectively. The probability of exceedance from the LS limit state under $S_a=0.9g$ for the EQ-Only, 1H+EQ, 2H+EQ, and 3H+EQ scenarios is 78%, 86%, 97%, and 100%, respectively. At $S_a=0.5g$, these values are 3%, 6%, 25%, and 51%, respectively. The probability of exceedance at the CP limit state for the same scenarios under $S_a=0.9g$ is 26%, 34%, 50%, and 74%, respectively, and under $S_a=1.3g$, these values are 63%, 75%, 84%, and 95%, respectively.

5.2. Second section: considering random variables

In the previous section, uncertainty was considered only for the seismic load during the deterministic analysis. Twenty-eight records with different spectral accelerations (S_a) were the only variables in that analysis. In this section, however, IDA curves are presented and examined using probabilistic methods, taking into account all the parameters listed in Table 4 as sources of uncertainty. Accordingly, all parameters in Table 4 are treated as a sample space, and probabilistic IDA curves are generated using the Monte Carlo method. The target coefficient of variation (COV) is set to 0.02, based on the study by Kim et al. [37]. Probabilistic IDA curves are calculated and presented as cumulative distribution function (CDF) curves at each spectral acceleration using the Monte Carlo approach, as depicted in Figure 15. To obtain each curve, a minimum of 4,000 analyses were performed to achieve the target COV of 0.02. In each graph of Figure 15, the only constant variable is the spectral acceleration (S_a), while all other parameters are treated as random variables. In the probabilistic method, a set of maximum drift values is presented cumulatively at each spectral acceleration. Each CDF curve represents the range of

variation of maximum drift values at a given spectral acceleration and the probability distribution they follow.

The results of the probabilistic analyses indicate that as the spectral acceleration of seismic loads increases, the CDF curves of the maximum structural drift span wider ranges. Furthermore, the longer the duration of fire exposure, the more the CDF curves shift toward higher values. For example, a 50% exceedance probability at $S_a = 1g$ corresponds to a maximum drift of 0.037 in the EQ-Only case. In contrast, for the 1H+EQ, 2H+EQ, and 3H+EQ cases, this value corresponds to maximum drifts of 0.041, 0.059, and 0.075, respectively. In other words, the mean drift at $S_a = 1g$ is 0.037 under only seismic loading and 0.075 in the 3H+EQ scenario. Probabilistic IDA curves provide considerably more information than deterministic IDA curves. For instance, it is straightforward to determine from these curves the probability of exceeding a drift value of 0.01 (the IO-level drift) for any scenario and at any spectral acceleration.

Figure 16 presents the range of inter-story drift variations for different scenarios at various spectral accelerations. In each scenario and for each spectral acceleration, the range represents the interval from the mean minus the standard deviation to the mean plus the standard deviation [36], with a wider range indicating a larger dispersion of maximum drift values. The results show that as spectral acceleration increases, the range of drift variations in the probabilistic analysis also increases, meaning the influence of uncertainties (random variables) becomes more pronounced in the EQ-Only, 1H+EQ, 2H+EQ, and 3H+EQ scenarios. Additionally, as expected, the mean drift values increase with spectral acceleration. The mean and standard deviation values for the considered scenarios are presented in Table 5. According to Figure 16, the width of the drift ranges in the 1H+EQ, 2H+EQ, and 3H+EQ scenarios is larger than in the EQ-Only case, indicating that the dynamic response of fire-damaged structures is more sensitive to variations in random variables compared to structures that have not been exposed to fire. Based on sensitivity analysis concepts, greater fluctuations correspond to higher sensitivity of the structure to random variables, so that the 3H+EQ scenario exhibits higher sensitivity than 2H+EQ, which is higher than 1H+EQ, which in turn is higher than EQ-Only. In summary, fire-induced damage reduces the seismic resistance of structures, as for a given spectral acceleration the structure experiences higher drift and approaches limit states, while also increasing sensitivity to uncertainties. According to Table 5 and Figure 16, the longer the duration of fire exposure, the higher the mean drift and the wider its variation at the same spectral acceleration.

Figure 17 presents the fragility curves obtained from the probabilistic method. The results of the probabilistic fragility analysis indicate that the probability of exceedance at the

Immediate Occupancy (IO) performance level at $S_a=0.5g$ is 40% in the EQ-Only case. For the 1H+EQ, 2H+EQ, and 3H+EQ cases, this probability rises to 51%, 72%, and 80%, respectively. The probability of exceedance at the Life Safety (LS) limit state at $S_a=0.9g$ is 71%, 86%, 90%, and 97% for the EQ-Only, 1H+EQ, 2H+EQ, and 3H+EQ cases, respectively. These values at $S_a=0.5g$ are 8%, 9%, 27%, and 48%, respectively. The probability of exceedance at the Collapse Prevention (CP) limit state for the aforementioned cases at $S_a=0.9g$ is 29%, 40%, 56%, and 68%, while at $S_a=1.3g$, it is 69%, 78%, 86%, and 90%, respectively. Therefore, it is evident that increasing the duration of fire exposure leads to higher exceedance probabilities at all limit states. Applying a seismic load with $S_a=0.9g$ to a frame damaged by three hours of fire exposure results in approximately a 39% increase in the exceedance probability at the CP limit state compared to a structure that has not experienced fire exposure.

Comparison of fragility curves obtained from deterministic and probabilistic methods illustrates that these curves have different values. The exceedance probability values derived from the probabilistic method are more accurate than those from the deterministic method due to the consideration of uncertainties and the considerable number of analyses in the probabilistic method.

6. Sensitivity Analysis

In this section, the sensitivity of the critical floor drift values to the random variables listed in Table [4] is examined using Monte Carlo simulation methods. In the previous probabilistic analysis, all parameters introduced in Table [4] were simultaneously considered as uncertainties to generate IDA curves. However, in this sensitivity analysis, to obtain the cumulative distribution function (CDF) curves from Monte Carlo simulations, all random variables are first fixed at their mean values. Then, one variable whose sensitivity is to be assessed is selected, and its corresponding values according to its probability distribution are defined as a sample space. A Monte Carlo simulation is subsequently performed using this sample space. This section will illustrate how variations in each random variable affect the maximum structural drift.

Using the Monte Carlo method, the cumulative distribution function (CDF) curves of the maximum drift values of the structure under the Northridge earthquake record were obtained for four scenarios: EQ-Only, 1H+EQ, 2H+EQ, and 3H+EQ. Figure 18 shows the CDF curves of the maximum floor drift values for the different fire exposure scenarios. At least 2,000 thermo-mechanical analyses were performed to extract each probabilistic CDF curve. Based on the study by Esfahani et al. [38], a coefficient of variation of 0.05 was assumed to ensure convergence in the probabilistic analysis. The output of the Monte

Carlo simulation, presented as CDF curves, indicates the sensitivity of each variable. The wider the CDF curve, the greater the sensitivity of the structural response to the corresponding random variable. For instance, in the EQ-Only scenario, the yield stress of the reinforcement has the greatest influence on the structural drift, as its curve is wider than those of other variables. In all cases, the curves for the modulus of elasticity, span length, and live load are narrower than those of the other variables, indicating that these variables exhibit the least sensitivity. In the 1H+EQ scenario under the Northridge earthquake record (Figure 18-b), the dead load shows the widest curve and the highest sensitivity among all variables. In the 2H+EQ scenario, under the same earthquake record, the thickness of the reinforcement cover exhibits the highest sensitivity. Finally, in the 3H+EQ scenario, the yield stress of the reinforcement has the greatest sensitivity.

Using cumulative distribution function (CDF) curves to evaluate the sensitivity of random variables can be somewhat challenging. Therefore, in various references, the value of two standard deviations of the results (the range between the mean plus the standard deviation and the mean minus the standard deviation) has been used as a measure of response fluctuations. Figure 19 presents the structural response fluctuations for each random variable in the EQ-Only, 1H+EQ, 2H+EQ, and 3H+EQ scenarios under the Northridge earthquake record. According to this figure, the highest fluctuation across all analyses corresponds to the yield stress variable in the 3H+EQ scenario under the Northridge earthquake record. The results indicate that random variables exhibit different levels of fluctuations under various loading conditions. In general, the sensitivity of random variables to structural drift increases with the duration of thermal loading. Furthermore, in different fire exposure scenarios (1H+EQ, 2H+EQ, and 3H+EQ), one random variable may have the greatest influence on structural drift in one scenario, while another parameter may dominate in a different scenario. For instance, in the EQ-Only scenario under the Northridge earthquake record, the yield stress shows the highest sensitivity. In the 1H+EQ and 2H+EQ scenarios under the same earthquake record, the dead load exhibits the greatest sensitivity, whereas in the 3H+EQ scenario, the yield stress again demonstrates the highest sensitivity. Overall, three parameters—yield stress, dead load, and concrete strength—exhibit the highest sensitivity. The concrete cover thickness also shows relatively high sensitivity in these scenarios due to its insulating role for the reinforcement.

Conclusion

In this study, the seismic fragility of reinforced concrete moment-resisting frames damaged by fire and without any strengthening was investigated using probabilistic and sensitivity analyses. To this end, a structure was first designed and then modeled with

thermo-mechanical properties in OpenSees. Three fire scenarios with heating and cooling phases, based on EN 1991-1-2, were defined, with the heating phase applied to the structure for one, two, and three hours. The beam and column sections of the fire-exposed floor were initially modeled and analyzed in Abaqus for heat transfer analysis. The output from Abaqus was then used to model and perform thermo-mechanical analysis in OpenSees. Subsequently, the considered frame was analyzed under four scenarios: without fire (EQ-Only), one-hour fire exposure (1H+EQ), two-hour fire exposure (2H+EQ), and three-hour fire exposure (3H+EQ), both with and without considering random variables, using Monte Carlo probabilistic analysis. The dynamic response, IDA curves, and fragility curves were then calculated. Finally, the sensitivity of the seismic response of the frame to random variables was evaluated.

Results of Deterministic Analysis (Without Considering Random Variables):

- If the structure is damaged by fire, the maximum drift increases. Therefore, the average maximum drift of the floors for EQ-Only, 1H+EQ, 2H+EQ, and 3H+EQ scenarios are 0.026, 0.029, 0.034, and 0.037, respectively.
- The hysteresis curves of reinforcement and concrete indicate that the longer the duration of thermal loading, the lower the resistance of concrete and reinforcement to seismic loads, and their behavior becomes more brittle with reduced strength. In the 3H+EQ scenario, the reinforcement strength is reduced by half. Moreover, the ultimate concrete strength occurs at higher strains.

Results of Probabilistic Analysis (Considering Random Variables):

- As the spectral acceleration increases, the range of drift variations in probabilistic analysis becomes larger. The dynamic response variations of the frame in 1H+EQ, 2H+EQ, and 3H+EQ scenarios are more sensitive to random variables compared to EQ-Only. Additionally, the longer the fire exposure duration, the greater the mean drift and its fluctuations at the same spectral acceleration.
- Comparison of fragility curves obtained from deterministic and probabilistic methods indicates that in both approaches, fire exposure increases the probability of exceeding limit states (IO, LS, CP) and reduces the seismic resistance of the frame. The longer the fire duration, the higher the exceedance probability at various performance levels under seismic loading. For example, the probability of exceeding the LS limit state at $S_a=0.9g$ for EQ-Only, 1H+EQ, 2H+EQ, and 3H+EQ is 78%, 86%, 97%, and 100% in the deterministic method, and 71%, 86%, 90%, and 97% in the probabilistic method, respectively.

- Comparing fragility curves from deterministic and probabilistic methods shows that exceedance probabilities from the probabilistic analysis are more accurate due to the consideration of uncertainties and the large number of simulations.

The results of the sensitivity analysis indicate that, in fire-damaged structures, the seismic response is most sensitive to dead load, reinforcement yield stress, concrete strength, and reinforcement cover among all considered parameters. Conversely, the modulus of elasticity of the reinforcement, span length, and live load exhibit the lowest sensitivity.

References

- [1] Lu, C.K., Chan, S.L., Zha, X.X. "Nonlinear pre-fire and post-fire analysis of steel frames", *Engineering structures*, 27(11), pp. 1689-1702 (2005). DOI:10.1016/j.engstruct.2005.06.003
- [2] Moradi, M., Tavakoli, H., Abdollahzadeh, G. "Probabilistic assessment of failure time in steel frame subjected to fire load under progressive collapses scenario", *Engineering failure analysis*, 102, pp. 136-147(2019). DOI:10.1016/j.engfailanal.2019.04.015
- [3] Ni, S., Birely, A.C. "Post-fire seismic behavior of reinforced concrete structural walls", *Engineering Structures*, 168, pp. 163-178(2018). DOI:10.1016/j.engstruct.2018.04.018
- [4] Xiao, J.-Z., Li, J., Huang, Z. F. "Fire response of high-performance concrete frames and their post-fire seismic performance", *ACI Structural Journal*, 105(5) , pp. 531(2008).
- [5] Kodur, V.K.R., Agrawal, A. "An approach for evaluating residual capacity of reinforced concrete beam exposed to fire", *Engineering Structures*, 110, pp. 293-306(2016). DOI:10.1016/j.engstruct.2015.11.047
- [6] Li, L. Z., Liu, X., Yu, J. T., et al. " Experimental study on seismic performance of post-fire reinforced concrete frames", *Engineering Structures*, 179, pp. 161-173 (2019). DOI:10.1016/j.engstruct.2018.10.080
- [7] Wang, G.Y., Zhang, C., Xu, J., et al. " Post-fire seismic performance of SRC beam to SRC column frames", *Structures*, 25, pp.323-334 (2020). DOI:10.1016/j.istruc.2020.03.01
- [8] Jia, Y. Q., Wang, C., Li, L. Z., et al. " Residual seismic performance of fire-damaged reinforced concrete frame structure with metallic yielding dampers", *Journal of Structural Engineering*, 148(4), pp. 04022003 (2022). DOI:10.1061/(ASCE)ST.1943-541X.0003284

- [9] Jin, L., Lan, D. Q., Zhang, R. B., et al. "Performance of RC beam-column assemblies during and after elevated temperature to resist progressive collapse", *Engineering Structures*, 283, pp. 115802 (2023). DOI:10.1016/j.engstruct.2023.115802
- [10] Sosso, B., Berke, P.Z. " Probabilistic investigation of reinforced concrete structures under fire loading accounting for material and geometric uncertainties", *Advances in Structural Engineering*, 26(7), pp. 1307-1324 (2023). DOI:10.1177/13694332221151019
- [11] Aydin, A. C., Bayrak, B., Alcan, H. G., et al. "Fire Performance of Steel Profiles Covered with Self Compacting Concrete", *Scientia Iranica*, 2023. DOI:10.24200/sci.2023.60188.6652
- [12] Van Cao, V., Trinh, T. M. N. "Performance of circular concrete filled steel tubes after fire exposure: experiments", *In Structures*, 55, pp. 1331-1341 (2023). DOI:10.1016/j.istruc.2023.06.110
- [13] Thongchom, C., Bui, L. V. H., Poonpan, N., et al. " Experimental and numerical investigation of steel-and GFRP-reinforced concrete beams subject to fire exposure", *Buildings*, 13(3), pp. 609 (2023). DOI:10.3390/buildings13030609
- [14] Liu, C., Wang, P., Lu, X., et al. "Residual flexural behaviour comparison between composite and monolithic beams after fire exposure", *Journal of Building Engineering*, 64, pp. 105584 (2023). DOI:10.1016/j.jobe.2022.105584
- [15] Li, J., Wang, W., Chen, P., et al. "Post-fire seismic performance of precast concrete columns with grouted sleeve connections: An experimental study", *In Structures*, 66, pp. 106816 (2024). DOI:10.1016/j.istruc.2024.106816
- [16] Chandra, S., Sharma, U. K., Green, M., et al. " Fire performance of corroded reinforced concrete columns", *Fire Technology*, 60(4), pp. 2265-2295 (2024). DOI:10.1007/s10694-023-01472-x
- [17] Wu, Z., Lu, X., Deng, B., et al. " Full-scale experiment on performance of damaged self-centering concrete joints after post-earthquake fire", *Journal of Building Engineering*, 99, pp. 111522 (2024). DOI:10.1016/j.jobe.2024.111522
- [18] Kunawisarut, A., Jongvivatsakul, P., Jirawattanasomkul, T., et al. "Strengthening fire-damaged concrete with jute fiber-reinforced biopolymer: Experimental investigation and sustainability assessment", *Construction and Building Materials*, 474, pp. 141081 (2025). DOI:10.1016/j.conbuildmat.2025.141081
- [19] Wang, W., Zhu, T., Gao, X., et al. "Fire Test on Insulated Steel Beams with Fire-Protection Coating and Fiber Cement Board", *Buildings*, 15(12), pp. 2121 (2025). DOI:10.3390/buildings15122121

- [20] Azadi Kenari, M., Abdollahzadeh, G., Hashemi, S. K. "Experimental and Numerical Post-Fire Seismic Performance Assessment of Recycled Aggregate Concrete Beam-Column Joints", Available at SSRN 5297128, (2025). DOI:10.2139/ssrn.5297128
- [21] Zhang, Y., Yuan, Z., Zhang, L., et al." Experimental and theoretical study of fire resistance of steel slag powder concrete beams", *Engineering Structures*, 325, pp. 119402 (2025). DOI:10.1016/j.engstruct.2024.119402
- [22] OpenSEES v. 3.3.0, 2021. Open system for earthquake engineering simulation, Pacific Earthquake Engineering Research Center, Available at: <http://opensees.berkeley.edu>
- [23] Asadi, I., Shafigh, P., Hassan, Z. F. B. A., et al." Thermal conductivity of concrete—A review", *Journal of Building Engineering*, 20, pp. 81-93(2018). DOI:10.1016/j.jobbe.2018.07.002
- [24] Moradi, M., Tavakoli, H., AbdollahZade, G. "Sensitivity analysis of the failure time of reinforcement concrete frame under postearthquake fire loading", *Structural Concrete*, 21(2), pp. 625-641 (2020). DOI:10.1002/suco.201900165
- [25] EN 1991-1-2. Design of composite steel and concrete structures—part 1-2: general rules-structural fire design, eurocodes. (2005).
- [26] Behnam, B." Failure sensitivity analysis of tall moment-resisting structures under natural fires", *International Journal of Civil Engineering*, 16(12), pp. 1771-1780 (2018). DOI:10.1007/s40999-017-0248-x
- [27] Dassault Systèmes, Abaqus 2020 Documentation, Providence, RI: Dassault Systèmes Simulia Corp, 2020.
- [28] Qiao, C. "Fire resistance of reinforced concrete restrained members during heating and cooling phases", Guangzhou: South China University of Technology, 2009.
- [29] Gernay, T., Franssen, J. M., Robert, F., et al. " Experimental investigation of structural failure during the cooling phase of a fire: Concrete columns", *Fire safety journal*, 134, pp. 103691 (2022). DOI:10.1016/j.firesaf.2022.103691
- [30] Moradi, M., Abdolmohammadi, M. " Seismic fragility evaluation of a diagrid structure based on energy method", *Journal of Constructional Steel Research*, 174, pp. 106311 (2020). DOI:10.1016/j.jcsr.2020.106311
- [31] Deniz, D., Song, J., Hajjar, J.F. " Energy-based seismic collapse criterion for ductile planar structural frames", *Engineering Structures*, 141, pp. 1-13 (2017). DOI:10.1016/j.engstruct.2017.02.051

- [32] Council, A.T., Quantification of building seismic performance factors.: US Department of Homeland Security, FEMA (2009).
- [33] FEMA 356, F.E., Prestandard and commentary for the seismic rehabilitation of buildings. Federal Emergency Management Agency: Washington, DC, USA, (2000).
- [34] Ramamoorthy, S.K., Gardoni, P., Bracci, J.M. " Probabilistic demand models and fragility curves for reinforced concrete frames", Journal of structural Engineering, 132(10), pp. 1563-1572 (2006). DOI:10.1061/(ASCE)0733-9445(2006)132:10(1563)
- [35] Wang, Y., Jiang, Y., Huang, Z., et al. " Post-fire behaviour of continuous reinforced concrete slabs under different fire conditions", Engineering structures, 226, pp.111342 (2021). DOI:10.1016/j.engstruct.2020.111342
- [36] Guo, Q., Jeffers, A.E. " Finite-element reliability analysis of structures subjected to fire", Journal of Structural Engineering, 141(4), pp. 04014129 (2015). DOI:10.1061/(ASCE)ST.1943-541X.0001082
- [37] Kim, J., Park, J.H., Lee, T.H. " Sensitivity analysis of steel buildings subjected to column loss", Engineering Structures, 33(2), pp. 421-432 (2011). DOI:10.1016/j.engstruct.2010.10.025
- [38] Esfahani, M., Hoseinzade, M., Shakiba, M., et al." Experimental investigation of residual flexural capacity of damaged reinforced concrete beams exposed to elevated temperatures", Engineering Structures, 240(4), pp.112388(2021). DOI:10.1016/j.engstruct.2021.112388

List of Figures:

- FIGURE 1. Flowchart of seismic analysis overall procedure in fire-damaged structures.
- FIGURE 2. Finite element model of the reinforced concrete frame.
- FIGURE 3. behavioral curve of material *ModIMKPeakOriented* [10].
- FIGURE 4. Temperature-time curve of the study [26].
- FIGURE 5. Finite element model of a reinforced concrete beam section in Abaqus for heat transfer analysis: a) one-hour, b) two-hour, c) three-hour thermal loading.
- FIGURE 6. Temperature-time curves of the beam cross-section: a) bottom reinforcement, b) concrete at the mid-section, c) concrete at the lowest section.

FIGURE 7. Experimental model of Qiao [28].

FIGURE 8. Comparison of the finite element model of the present study with Qiao's results: a) fire load curve and temperature-time curve at the mid-section, b) beam response curves under fire loading.

FIGURE 9. Experimental model by Gernay et al., b) cross-section of the reinforced concrete column [29].

FIGURE 10. a) Gernay model fire load curve, b) column validation results.

FIGURE 11. Maximum inter-story drift curves under earthquake loading.

FIGURE 12. Hysteresis curves of steel and concrete material of the beam: a) concrete, b) reinforcement.

FIGURE 13. IDA curves under deterministic scenarios: a) EQ-Only, b) 1H+EQ, c) 2H+EQ, d) 3H+EQ.

FIGURE 14. Fragility curves under various scenarios in a) IO, b) LS, c) CP limit states.

FIGURE 15. CDF curves resulted from probabilistic analyses in a) EQ-Only, b) 1H+EQ, c) 2H+EQ, d) 3H+EQ.

FIGURE 16. Variations of structural drift in different scenarios and spectral accelerations.

FIGURE 17. Fragility curves obtained from the probabilistic method: a) IO, b) LS, c) CP.

FIGURE 18. The results from the Monte Carlo analysis a) EQ-Only, b) 1H+EQ, c) 2H+EQ, d) 3H+EQ.

FIGURE 19. Variations resulted from the Monte Carlo analysis based on the response of Northridge earthquake.

List of Tables:

TABLE 1. Structural sections of the reinforced concrete frame.

TABLE 2. Behavioral model of concrete and steel in the OpenSees software [24]

TABLE 3. Seismic loadings [32].

TABLE 4. Specifications of random variables [17, 36, 37].

TABLE 5. Mean values and deviations of drift resulted from probabilistic analysis in different scenarios and spectral accelerations.

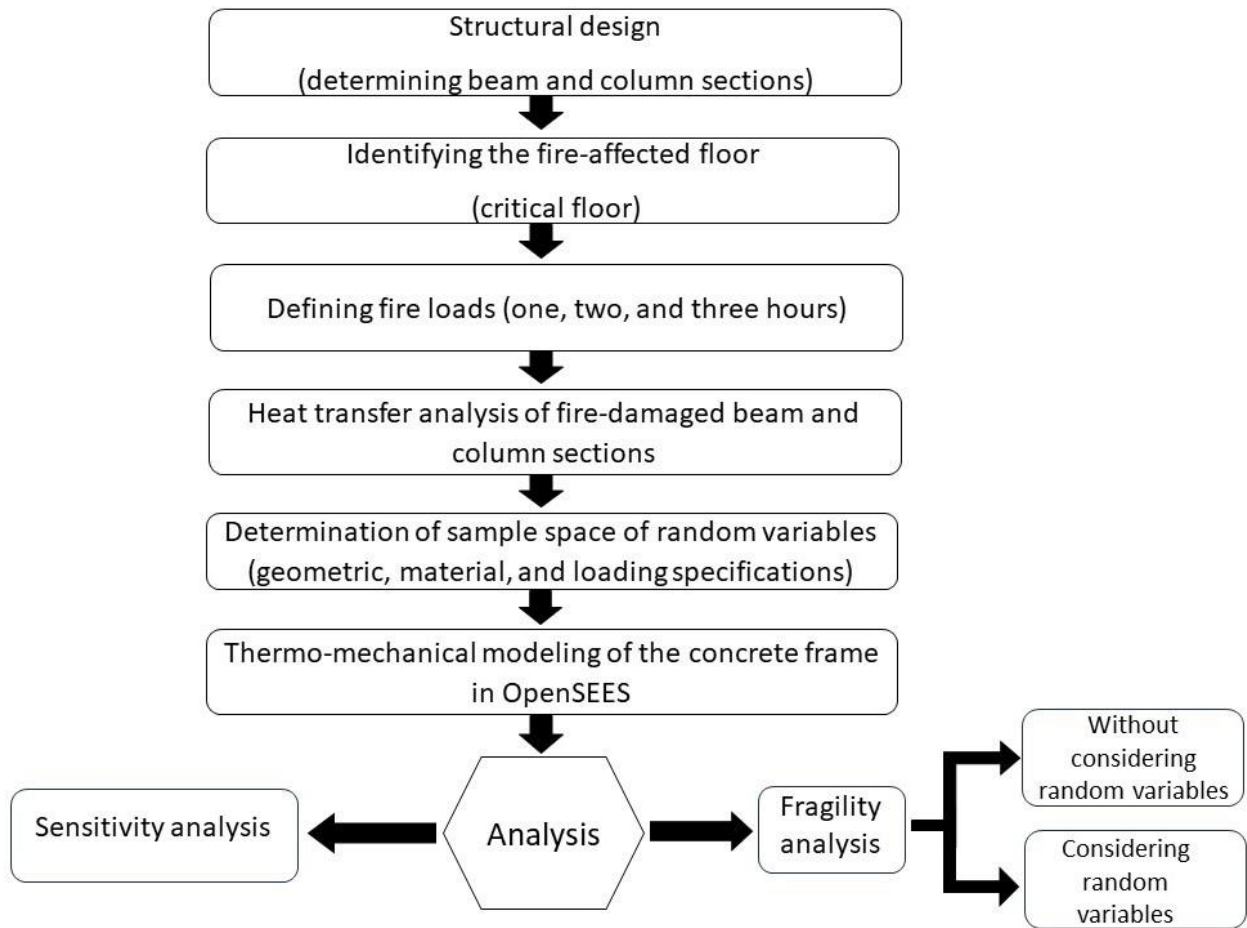


Figure 1. Flowchart of seismic analysis overall procedure in fire-damaged structures.

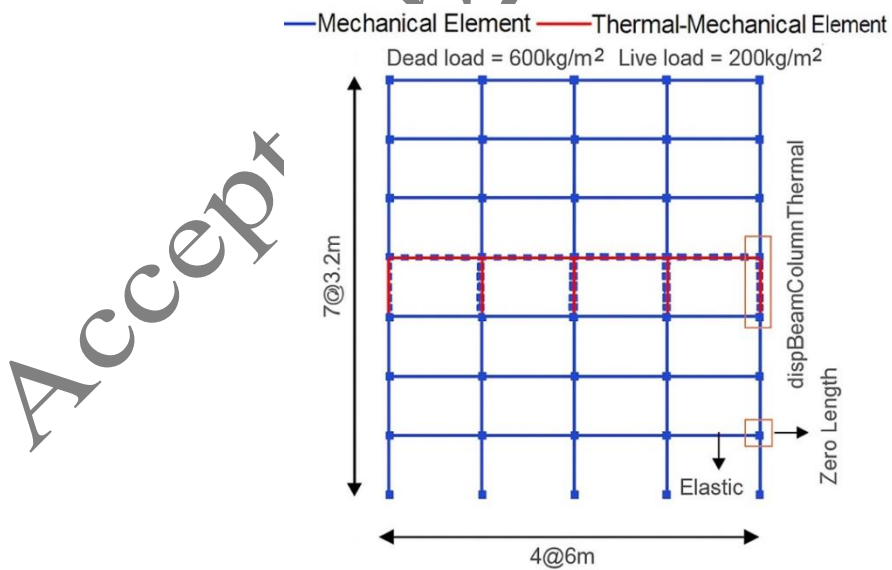


Figure 2. Finite element model of the reinforced concrete frame.

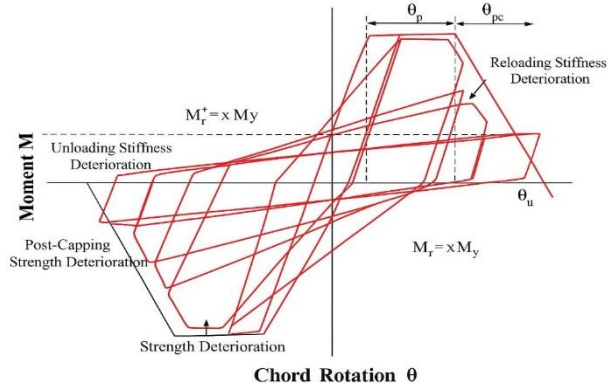


Figure 3. behavioral curve of material *ModIMKPeakOriented* [10].

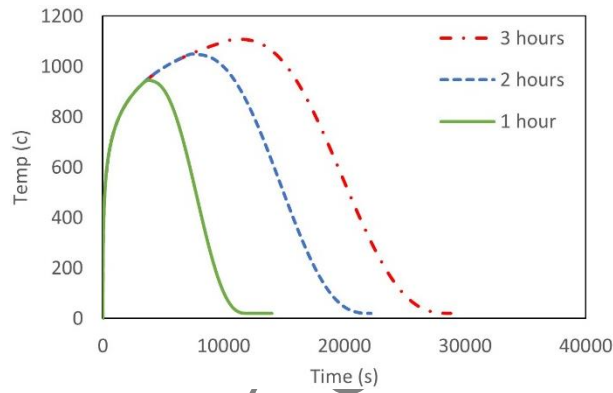
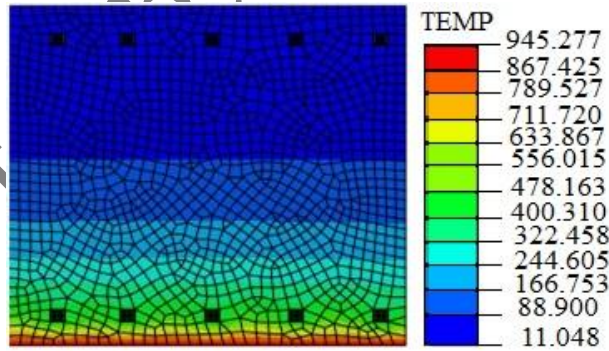
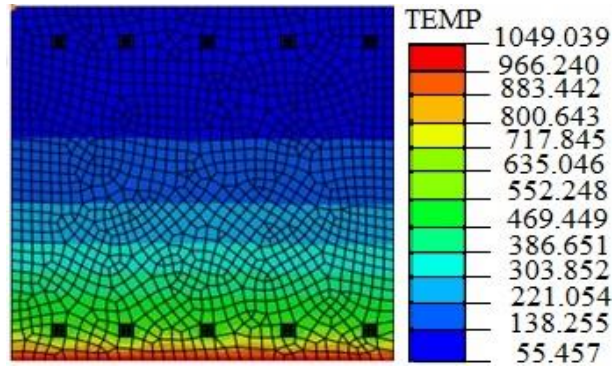


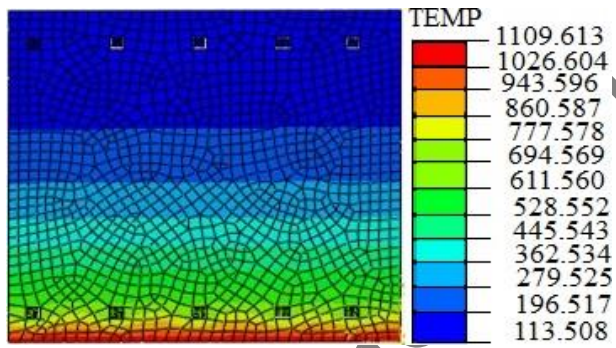
Figure 4. Temperature-time curve of the study [26].



a

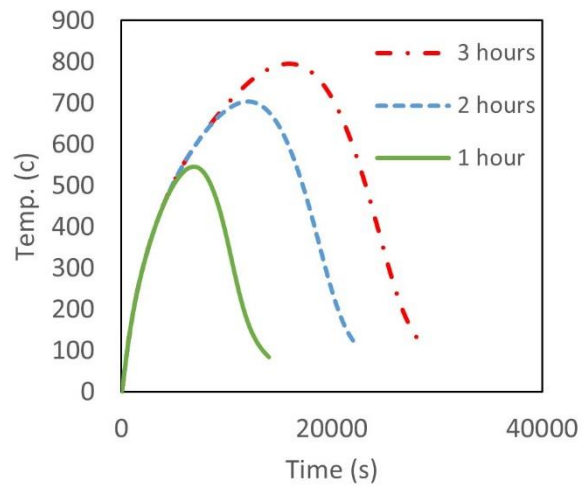


b

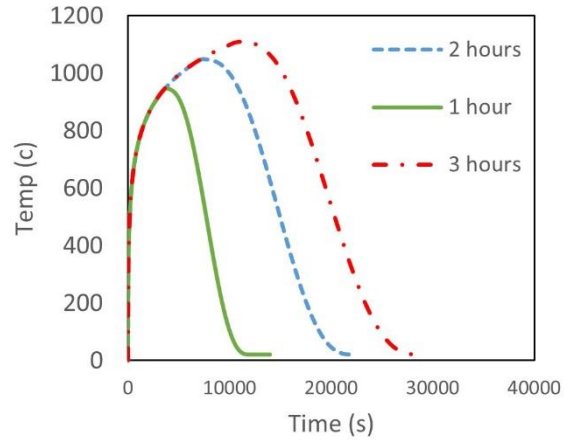


c

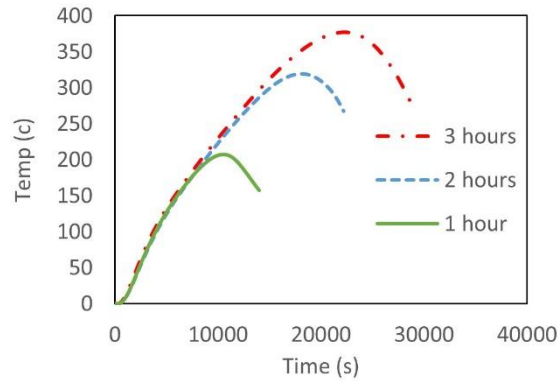
Figure 5. Finite element model of a reinforced concrete beam section in Abaqus for heat transfer analysis: a) one-hour, b) two-hour, c) three-hour thermal loading.



a



b



c

Figure 6. Temperature-time curves of the beam cross-section: a) bottom reinforcement, b) concrete at the mid-section, c) concrete at the lowest section.

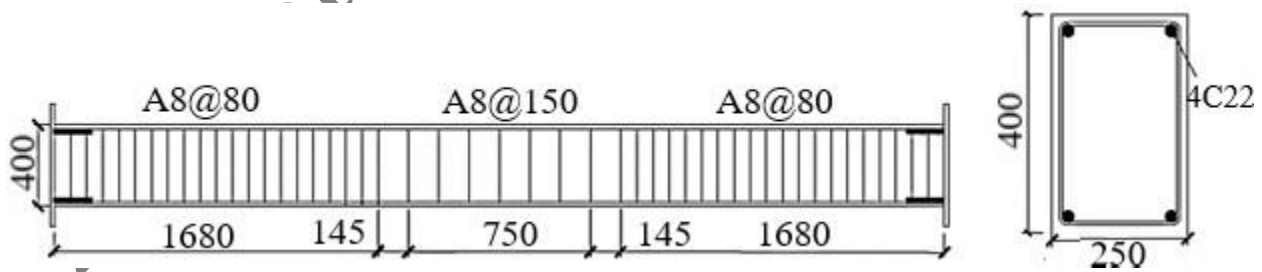
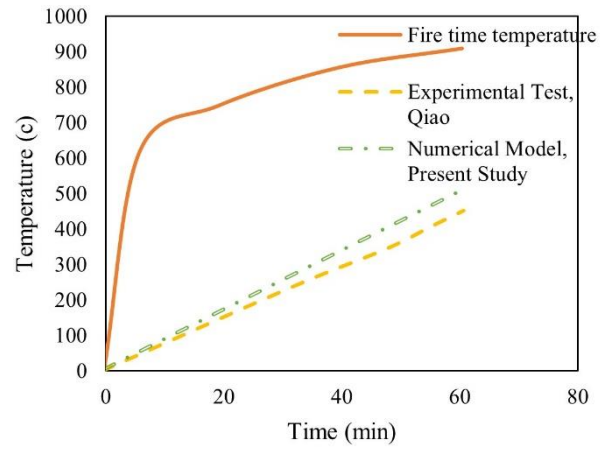
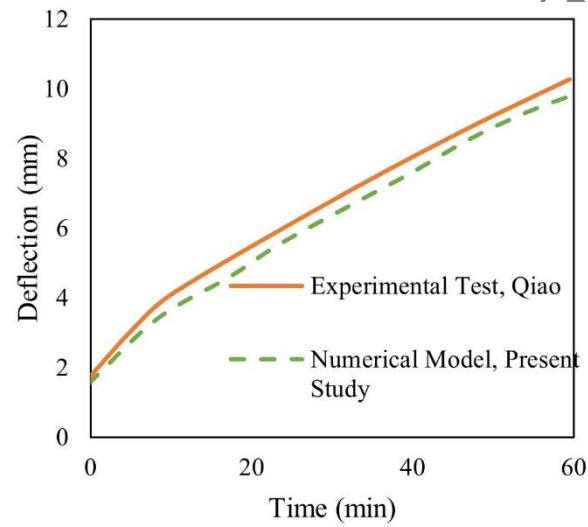


Figure.7. Experimental model of Qiao [28]

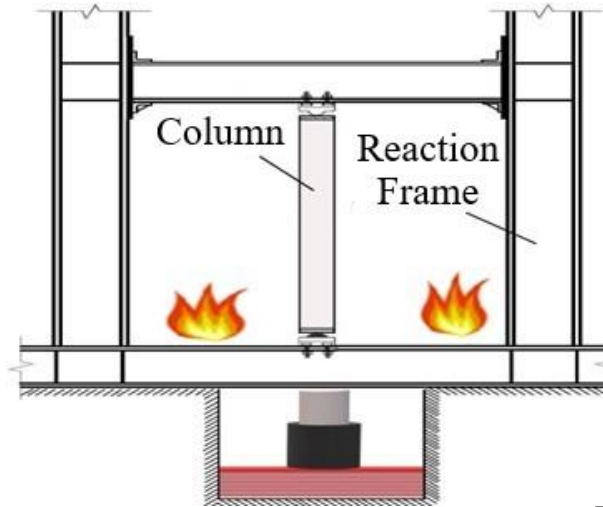


a

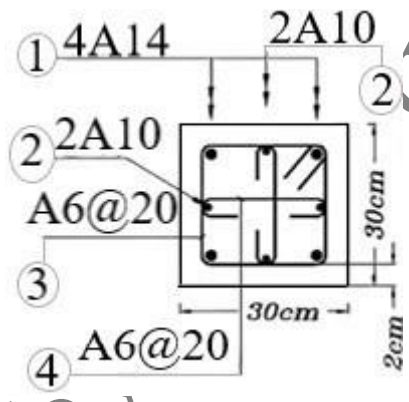


b

Figure 8. Comparison of the finite element model of the present study with Qiao's results: a) fire load curve and temperature-time curve at the mid-section, b) beam response curves under fire loading.

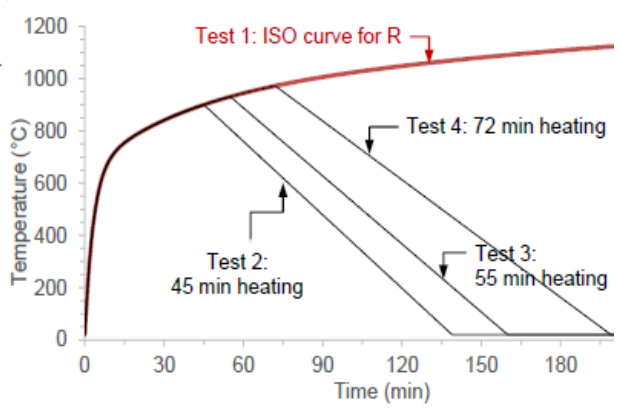


a

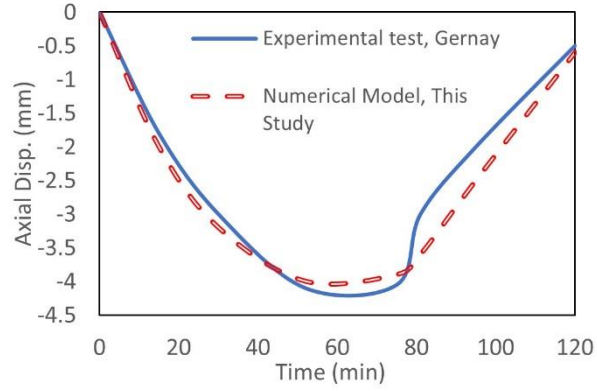


b

Figure 9. a) Experimental model by Gernay et al., b) cross-section of the reinforced concrete column [29].



a



b

Figure 10: a) Gernay model fire load curve, b) column validation results.

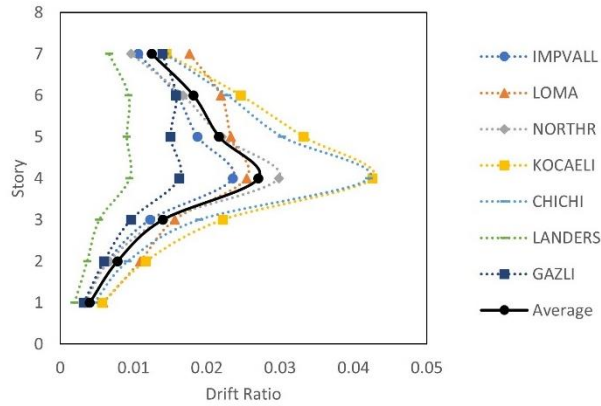
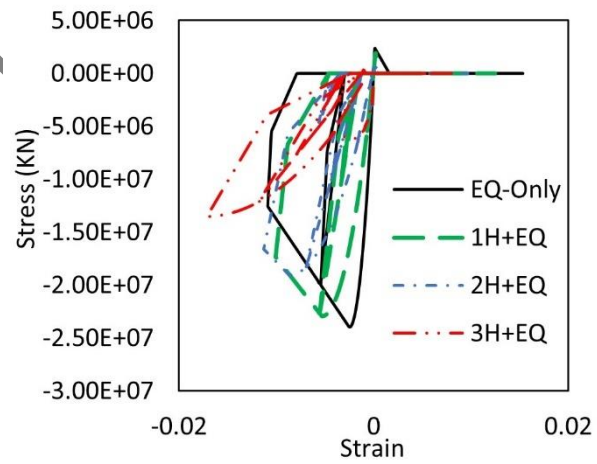
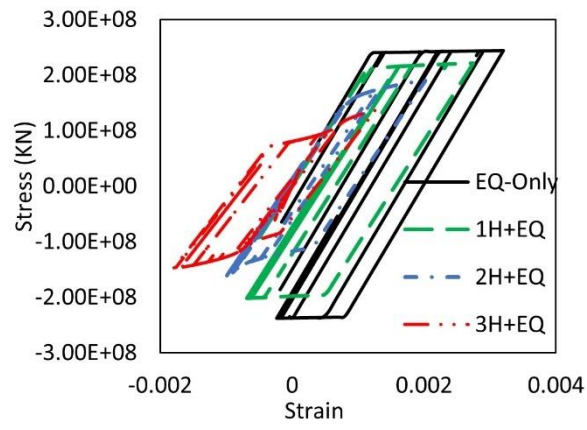


Figure 11. Maximum inter-story drift curves under earthquake loading.

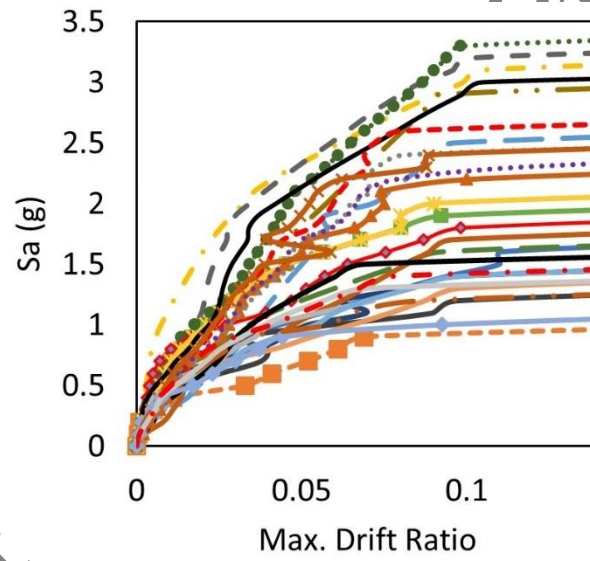


a



c

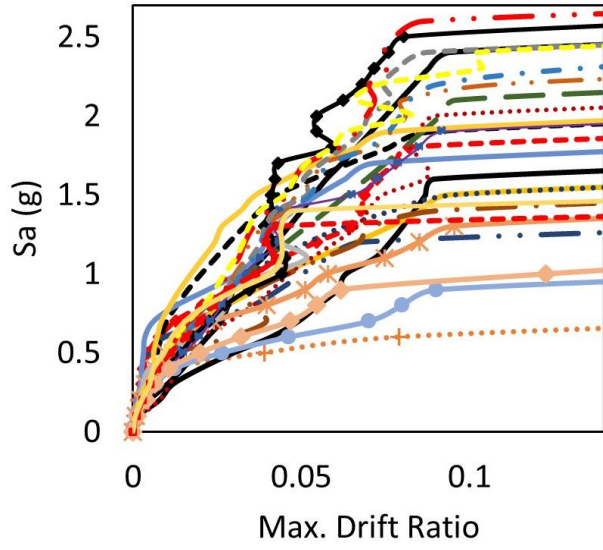
Figure 12. Hysteresis curves of steel and concrete material of the beam: a) concrete, b) reinforcement.



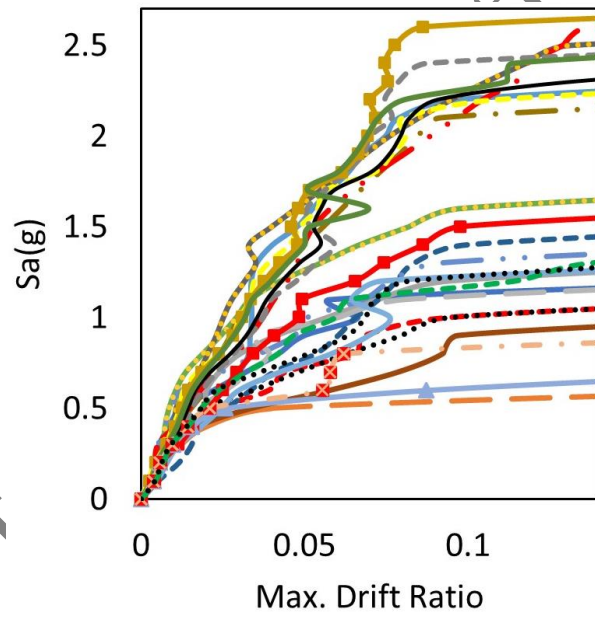
a

Accept

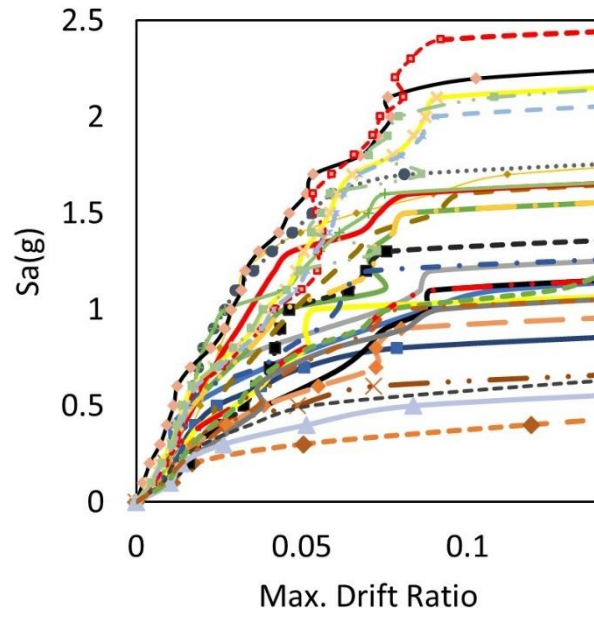
Iranica



b

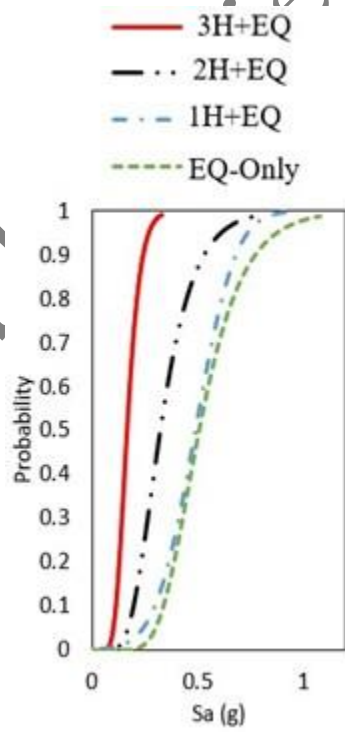


c

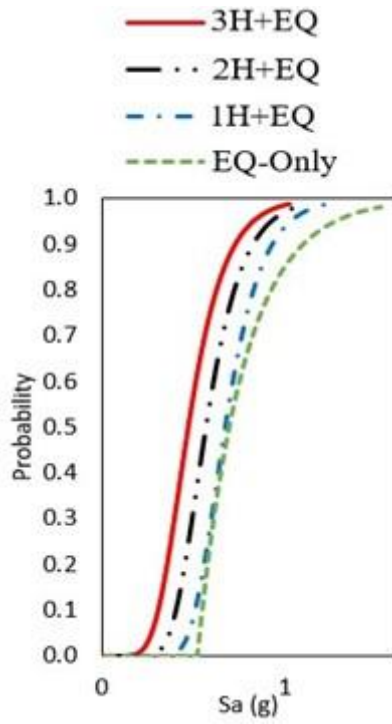


d

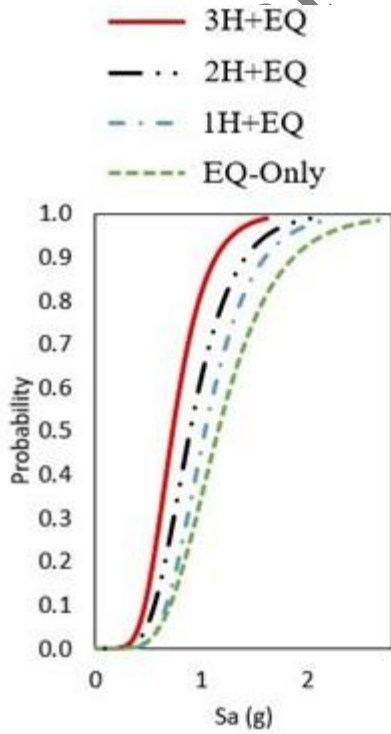
Figure 13. IDA curves under deterministic scenarios: a) EQ-Only, b) 1H+EQ, c) 2H+EQ, d) 3H+EQ.



a

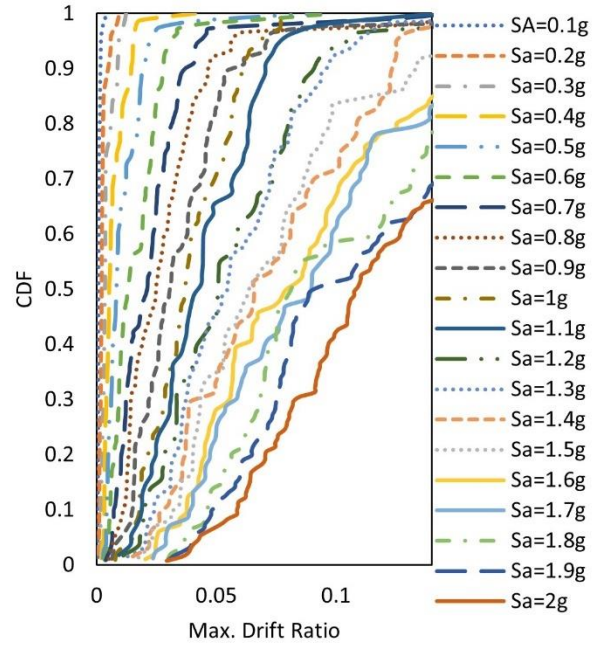


b

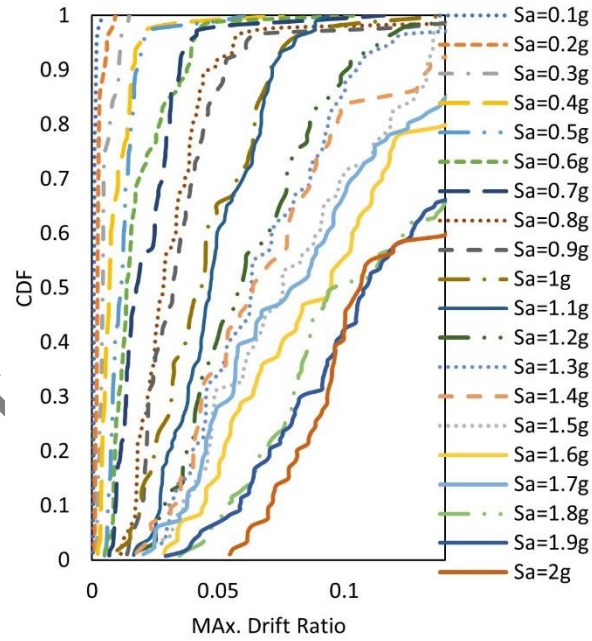


c

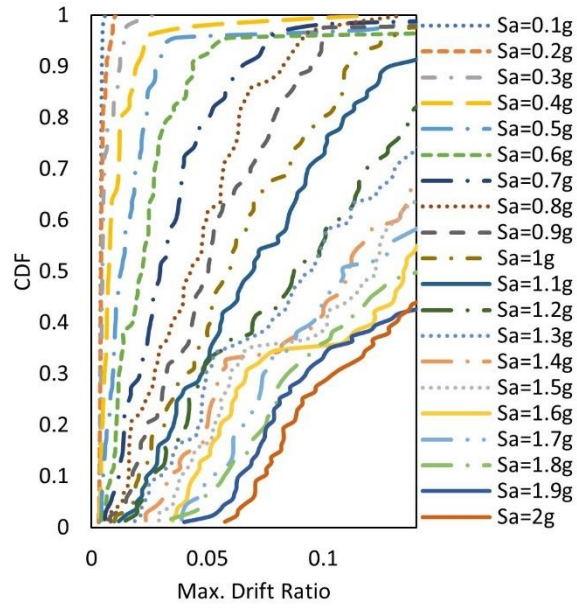
Figure 14. Fragility curves under various scenarios in a) IO, b) LS, c) CP limit states.



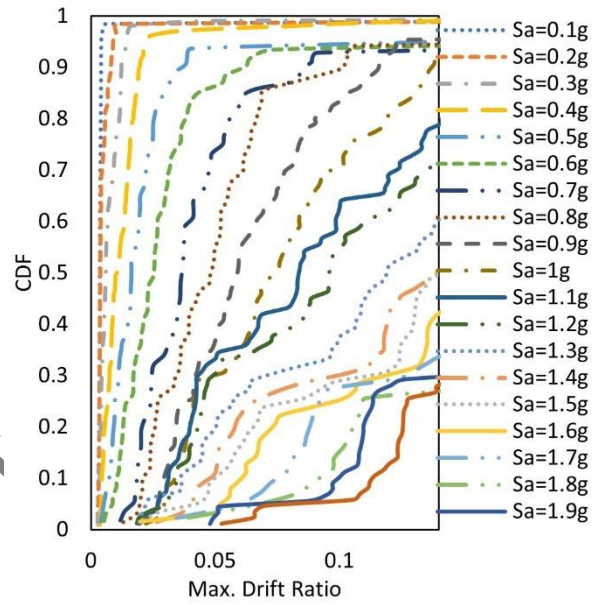
a



b



c



d

Figure 15. CDF curves resulted from probabilistic analyses in a) EQ-Only, b) 1H+EQ, c) 2H+EQ, d) 3H+EQ.

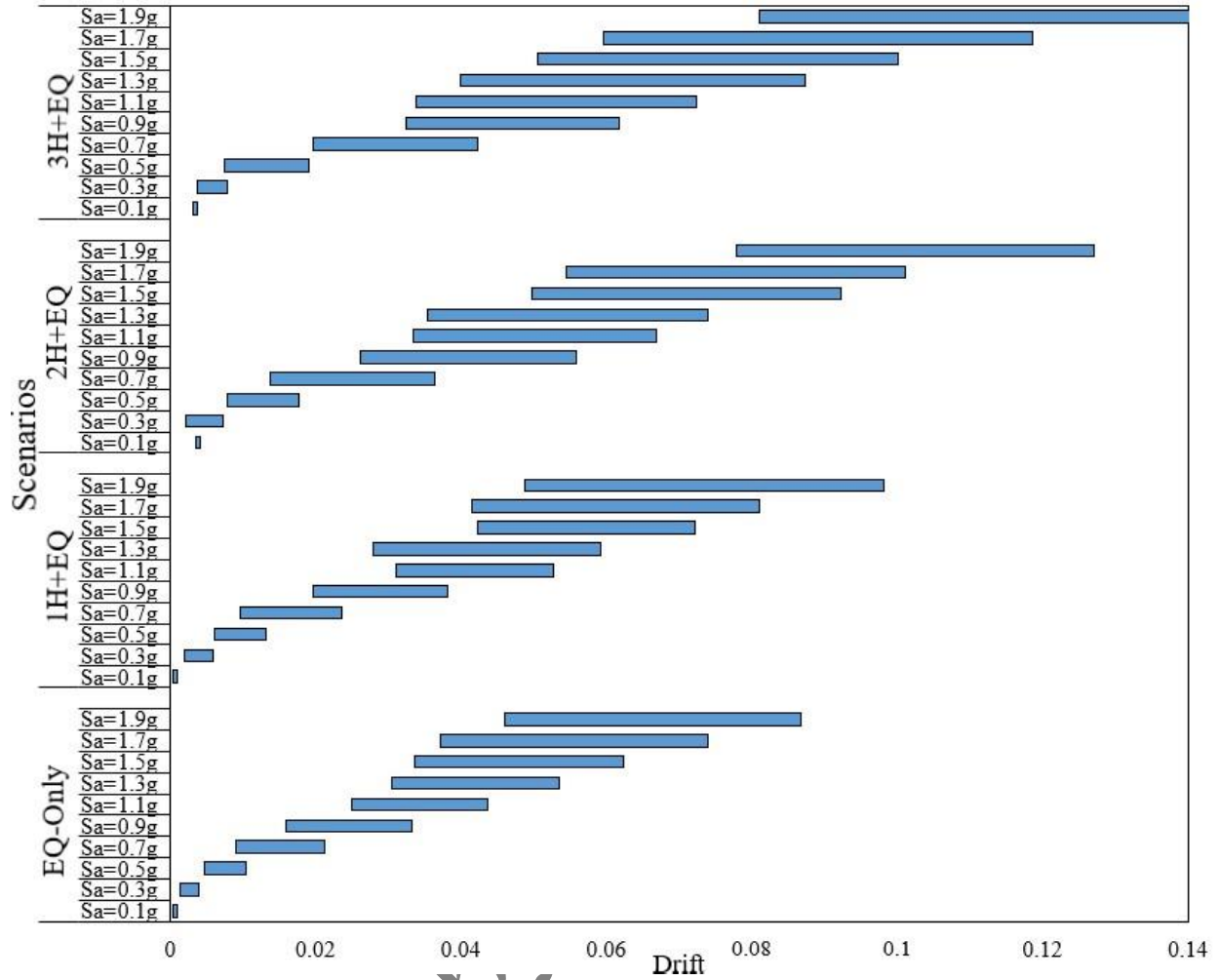
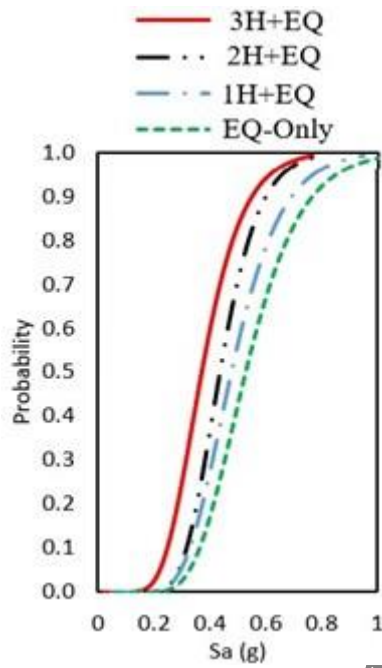
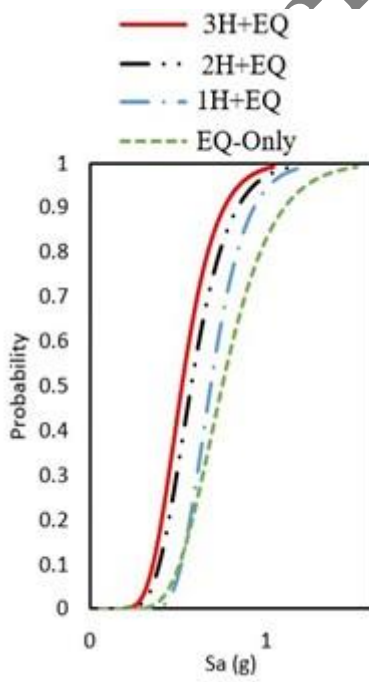


Figure 16. Variations of structural drift in different scenarios and spectral accelerations.

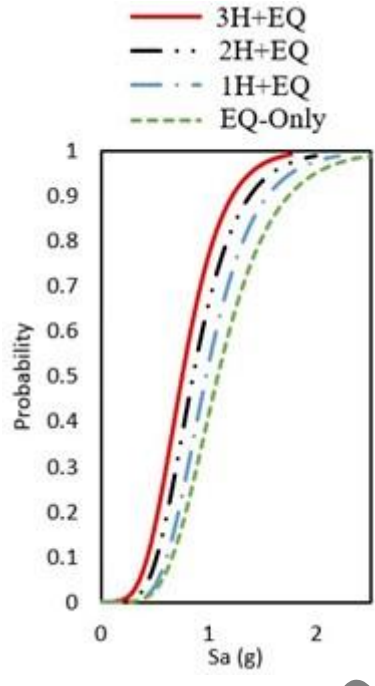
Accepted



a

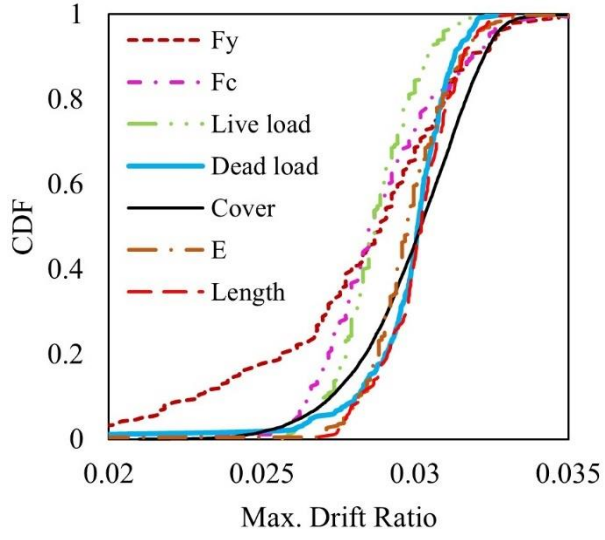


b

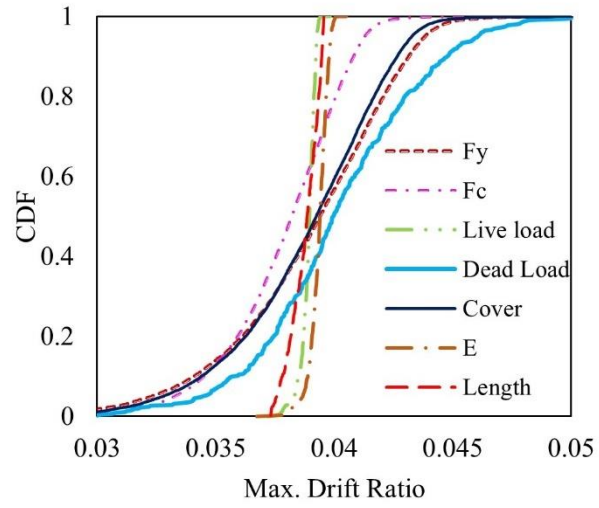


c

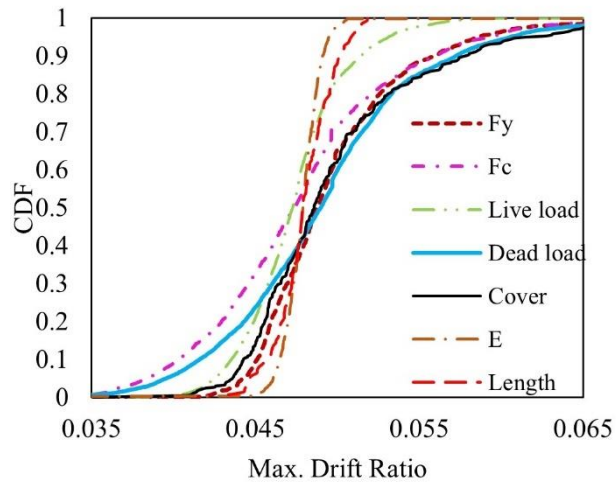
Figure 17. Fragility curves obtained from the probabilistic method: a) IO, b) LS, c) CP.



a



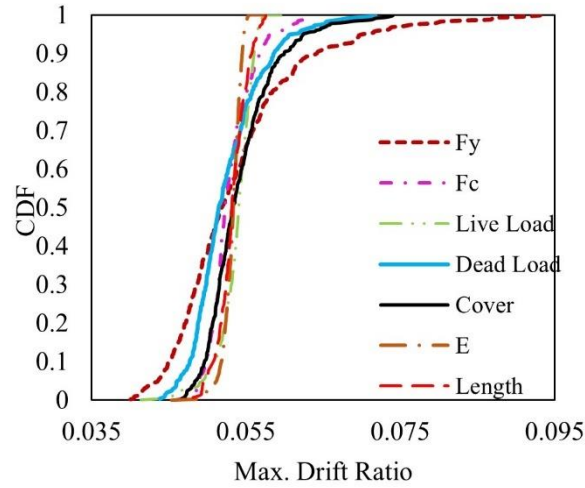
b



c

Accepted

Iranica



c

Figure 18. The results from the Monte Carlo analysis a) EQ-Only, b) 1H+EQ, c) 2H+EQ, d) 3H+EQ.

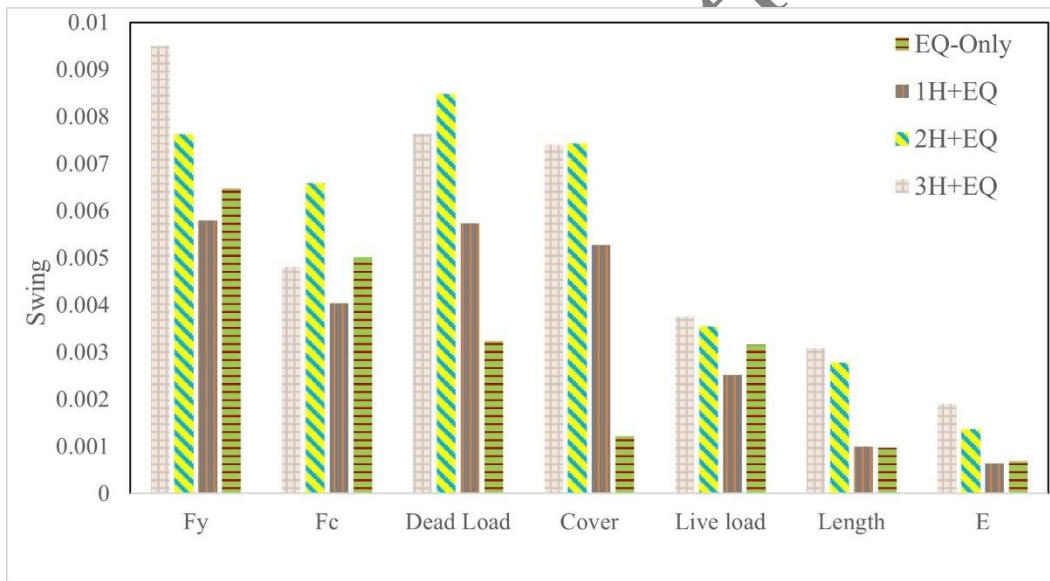


Figure 19. Variations resulted from the Monte Carlo analysis based on the response of Northridge earthquake.

Table 1. Structural sections of the reinforced concrete frame.

Story	Beam			Column	
	H	Bottom Rebar	Top Rebar	H	Rebar
1	50	8 T22	7 T22	70	22 T22
2	45	7 T20	6 T20	65	20 T20
3	45	6 T18	6 T18	55	20 T18
4	40	5 T16	5 T16	50	20 T18

5	40	5 T12	5 T 16	45	18 T18
6	35	5 T12	4 T 14	40	16 T16
7	35	5T12	4 T14	35	12 T16

Table 2. Behavioral model of concrete and steel in the OpenSees software [24].

<i>Concrete02thermal</i>				<i>Steel02thermal</i>		
$\theta(^{\circ}C)$	$f_{c,\theta} / f_{ck}$	$\epsilon_{c,\theta}$	$\epsilon_{cu,\theta}$	$f_{sy,\theta} / f_{yk}$	$f_{sp,\theta} / f_{yk}$	$E_{s,\theta} / E_s$
20	1	0.0025	0.02	1	1	1
100	1	0.004	0.0225	1	0.96	1
200	0.95	0.0055	0.025	1	0.92	0.87
300	0.85	0.007	0.0275	1	0.81	0.72
400	0.75	0.01	0.03	0.94	0.63	0.56
500	0.6	0.015	0.0325	0.67	0.44	0.4
600	0.45	0.025	0.035	0.4	0.26	0.24
700	0.3	0.025	0.0375	0.12	0.08	0.08
800	0.15	0.025	0.04	0.11	0.06	0.06
900	0.08	0.025	0.0425	0.08	0.05	0.05
1000	0.04	0.025	0.045	0.05	0.03	0.03
1100	0.01	0.025	0.0475	0.03	0.02	0.02

Table 3. Seismic loadings [32].

ID No.	Lowest Freq (Hz.)	PEER. NGA Record information		PGAmax (g)	PGVmax (cm/s.)
		FN Component	FP Component		
1	0.13	IMPVALL/H-E06_233	IMPVALL/H-E06_323	0.44	111.9
2	0.13	IMPVALL/H-E07_233	IMPVALL/H-E07_323	0.46	108.9
3	0.16	ITALY/A-STU_223	ITALY/A-STU_313	0.31	45.5
4	0.15	SUPERST/B-PTS_037	SUPERST/B-PTS_127	0.42	106.8
5	0.13	LOMAP/STG_038	LOMAP/STG_128	0.38	55.6
6	0.13	ERZIKAN/ERZ_032	ERZIKAN/ERZ_122	0.49	95.5
7	0.07	CAPEMEND/PET_260	CAPEMEND/PET_350	0.63	82.1
8	0.10	LANDERS/LCN_239	LANDERS/LCN_329	0.79	140.3
9	0.11	NORTHR/RRS_032	NORTHR/RRS_122	0.87	167.3
10	0.12	NORTHR/SYL_032	NORTHR/SYL_122	0.73	122.8
11	0.13	KOCAELI/IZT_180	KOCAELI/IZT_270	0.22	29.8
12	0.08	CHICHI/TCU065_272	CHICHI/TCU065_002	0.82	127.7
13	0.06	CHICHI/TCU102_278	CHICHI/TCU102_008	0.29	106.6
14	0.10	DUZCE/DZC_172	DUZCE/DZC_262	0.52	79.3
15	0.06	GAZLI/GAZ_177	GAZLI/GAZ_267	0.71	71.2
16	0.13	IMPVALL/H-BCR_233	IMPVALL/H-BCR_323	0.76	44.3
17	0.06	IMPVALL/H-CHI_233	IMPVALL/H-CHI_323	0.28	30.5
18	0.13	NAHANNI/S2_070	NAHANNI/S2_160	0.45	34.7
19	0.13	NAHANNI/S1_070	NAHANNI/S1_160	1.18	43.9
20	0.13	LOMAP/BRN_038	LOMAP/BRN_128	0.64	55.9
21	0.25	LOMAP/CLS_038	LOMAP/CLS_128	0.51	45.5
22	0.07	CAPEMEND/CPM_260	CAPEMEND/CPM_350	1.43	119.5

23	0.12	NORTHR/0637_032	NORTHR/0637_122	0.73	70.1
24	0.13	NORTHR/STC_032	NORTHR/STC_122	0.42	3.2
25	0.09	KOCAELI/YPT_180	KOCAELI/YPT_270	0.31	73
26	0.04	CHICHI/TCU067_285	CHICHI/TCU067_015	0.56	91.8
27	0.25	CHICHI/TCU084_271	CHICHI/TCU084_001	1.16	115.1
28	0.03	DENALI/ps10_199	DENALI/ps10_289	0.33	126.4

Table 4. Specifications of random variables [17, 36, 37].

Category	Item	Property	Mean	COV (%)	Dist'n type
Materials	Rebare	F_y	400 Mpa	10	Lognormal
	Rebare	E	2e5 Mpa	5	Normal
	Concrete	F_c	21 Mpa	10	Lognormal
Load	Dead Load		3000 Kg/m	10	Normal
	Live Load		1000 Kg/m	80	Gamma
Geometry	Dimension	Span Lenth	6 m	5	Gamma
	Cover	Cover Size	5 cm	40	Uniform

Table 5. Mean values and deviations of drift resulted from probabilistic analysis in different scenarios and spectral accelerations.

	EQ-Only		1H+EQ		2H+EQ		3H+EQ	
	Average	STD	Average	STD	Average	STD	Average	STD
Sa=0.1g	0.0009	0.0006	0.0009	0.0006	0.0039	0.0004	0.0037	0.0005
Sa=0.3g	0.0040	0.0026	0.0052	0.0032	0.0064	0.0042	0.0071	0.0035
Sa=0.5g	0.0104	0.0058	0.0120	0.0060	0.0160	0.0081	0.0172	0.0098
Sa=0.7g	0.0212	0.0122	0.0212	0.0117	0.0327	0.0189	0.0385	0.0189
Sa=0.9g	0.0333	0.0174	0.0351	0.0154	0.0508	0.0247	0.0568	0.0245
Sa=1.1g	0.0437	0.0186	0.0490	0.0179	0.0612	0.0278	0.0659	0.0322
Sa=1.3g	0.0534	0.0229	0.0539	0.0261	0.0675	0.0321	0.0795	0.0396
Sa=1.5g	0.0623	0.0287	0.0672	0.0250	0.0852	0.0354	0.0918	0.0412
Sa=1.7g	0.0739	0.0367	0.0744	0.0328	0.0932	0.0388	0.1088	0.0492
Sa=1.9g	0.0867	0.0407	0.0898	0.0410	0.1188	0.0410	0.1314	0.0505

Biographies:



Sajjad Mohammadian Abi is currently a Ph.D. candidate in Structural Engineering at the Islamic Azad University, Science and Research Branch, Tehran, Iran. He is a structural design engineer with experience in the design and analysis of reinforced concrete and steel structures. His research interests include the assessment and retrofitting of damaged structures, evaluation of post-fire performance of reinforced concrete structures, and probabilistic and reliability-based analysis of structural systems. He has authored and co-authored several research papers in the field of performance-based earthquake engineering and fire-structure interaction.



Mohammad Reza Mansoori received his B.Sc. degree in Civil Engineering from the University of Tehran in 2001, and his M.Sc. degree in Structural Engineering from the University of Tehran in 2004. He obtained his Ph.D. in Earthquake Engineering from the International Institute of Earthquake Engineering and Seismology (IIEES) in 2009. He is currently an Assistant Professor in the Department of Structural and Earthquake Engineering at the Islamic Azad University, Science and Research Branch, Tehran. His research interests include structural engineering, earthquake engineering, and seismic performance



Panam Zarfam received his PhD of Structure Engineering from Sharif University. He is a Professor in Civil Engineering at the Department of Structural Engineering, Science and Research Branch of Islamic Azad University where he has taught several graduate and undergraduate courses and supervised many PhD and master students. His areas of research include structure design, nonlinear analysis, seismic design, and active and semi-active control.